Hindawi
Mathematical Problems in Engineering
Volume 2018, Article ID 8740872, 17 pages
https://doi.org/10.1155/2018/8740872

*Research Article*

# A Method for Improving UWB Indoor Positioning

**Zhanjun Hao,[1,2] Beibei Li,[1] and Xiaochao Dang[1,2]**

[1]*College of Computer Science and Engineering, Northwest Normal University, Lanzhou 730070, China*
[2]*Gansu Province Internet of Things Engineering Research Center, Lanzhou 730070, China*

Correspondence should be addressed to Xiaochao Dang; dangxc@nwnu.edu.cn

Received 19 August 2018; Accepted 16 October 2018; Published 12 December 2018

Academic Editor: Filippo Cacace

Copyright © 2018 Zhanjun Hao et al. This is an open access article distributed under the Creative Commons Attribution License, which permits unrestricted use, distribution, and reproduction in any medium, provided the original work is properly cited.

The existing positioning methods that use received signal strength indication (RSSI) and channel state information (CSI) may suffer from multipath and shadowing in a complex wireless environment, which can result in more positioning errors. This paper proposes a method for accurate multilabel positioning in the non-line-of-sight (NLOS) environment. First, the position is roughly estimated using the orthogonal variable spreading factor (OVSF-TH) algorithm, which can automatically match the signal interference. The ultra-wideband (UWB) spectral density and pulse amplitude in the time domain are used to determine the direction of the label and enhance estimation of the mobile label direction. Then, the location of the tag is obtained by triangulation, and a coordinate-based coordinate estimation method is proposed to calculate the relative displacement of multiple tags to determine the label position. Finally, by setting up a real experimental environment, the influence of the number of base stations on the accuracy and the performance of the localization method under different circumstances are analyzed. The theoretical analysis and experimental results show that the method is simple to deploy, inexpensive, and very accurate in terms of positioning, having a clearly effective indoor positioning accuracy. Compared with other existing positioning methods, this method can achieve more accurate positioning. Moreover, it has important theoretical and practical applicability because of the reliability and accuracy of indoor positioning in an NLOS environment.

## 1. Introduction

The use of ultra-wideband (UWB) signals to locate objects in indoor complex multipath environments has the advantages of high positioning accuracy, strong anti-interference, and low power consumption. UWB signals are widely used in military, logistics, security, medical, search, rescue, and other applications [1]. Currently, UWB positioning technology is mainly based on time-of-arrival (TOA) algorithms, such as the maximum likelihood estimation algorithm [2], the threshold crossing (TC) threshold search algorithm [3], and the decoupled multiuser ranging (DEMR) algorithm [4]. The use of these algorithms to achieve positioning requires at least three base stations, with each base station accurately synchronized to the same time, which may increase the cost of the system.

UWB technology using nanosecond narrow pulses has sufficient bandwidth [5] and strong multipath resolution and is increasingly used in indoor positioning systems [6]. At the receiving end, if the direct path (DP) is accurately identified, the TOA of a signal can also be accurately estimated [7]. However, in a dense multipath propagation environment, especially in an indoor environment, the line-of-sight (LOS) path between a reference tag and the tag to be tested is blocked due to the influence of the non-line-of-sight (NLOS) signal. This signal is difficult to accurately estimate, reducing the accuracy of ranging and positioning [8]. If there is no DP at the transmitting and receiving ends, the signal will introduce more cost in the propagation process, resulting in an NLOS error [9]. Therefore, eliminating the influence of NLOS errors is crucial to improve the ranging and positioning accuracy [10]. The research on eliminating the effects of NLOS has mainly focused on two aspects: NLOS identification and NLOS error elimination [11]. If the received signal is known to originate from either an LOS or NLOS environment prior to processing, the positioning accuracy can be improved [12]. If the received signal is from an LOS environment, then it can be addressed without any processing, and the estimated value of the ranging can be directly obtained; hence, a more accurate tag position

estimation can be obtained directly [13]. If the received signal is from an NLOS environment, the received signal can be eliminated or mitigated for NLOS error processing, or the signal from the NLOS environment can be discarded before continuing to carry out positioning [14]. The existing algorithms for distinguishing between LOS and NLOS can be roughly divided into two types: algorithms based on ranging estimation and algorithms based on channel statistics [15].

The work in [16] proposed a noise-tolerant localization approach based on low-rank matrix completion called LoMaC. It addresses the problem of robust localization in WSNs. But LoMaC is an inherently centralized algorithm, which may not be suitable for large-scale networks. Reference [17] explored the problem of data missing and noise interference in wireless sensor networks localization. Then it gives a noise-tolerant WSNs localization method via multinorm regularized matrix completion named LMRMC. However, its proposed LMRMC is essentially a centralized localization approach, constrained by the computational efficiency and storage scale.

In view of the problems raised in the above references, this paper focuses on the accurate multilabel positioning method in the NLOS environment. UWB has the advantages of high positioning accuracy and close positioning distance, and the OVSF-TH method is used to adjust the waveform, which shows better communication quality and effectively avoids cluster burst errors that occur during node communication. In addition, after ensuring the stability of the node communication, the three-sided measurement method is used to obtain more stable coordinate data, thereby ensuring more accurate positioning data. The main contributions and research content of this paper are as follows:

(i) An UWB signal is used to determine the label position. Unlike the existing methods based on received signal strength and UWB, UWB indoor positioning provides more information for expressing UWB signals, making more accurate and practical tag positioning possible.

(ii) Even when an object is located between the deployed base station and a tag, the proposed method successfully captures the spectral density of the UWB signal and the "blocking" effect of the pulse position. This important phenomenon is used to determine the direction of the tag.

(iii) This article identifies the direction of a tag by statistically analyzing the UWB spectral density and the blocking effect of the pulse position. Using the detected UWB spectral density, the relevant receiving techniques, pulse position modulation, and code division multiple access methods are studied. By using the UWB pulse frequency domain, the variance and correlation of the pulse difference are calculated. At the same time, a strategy for improving the positioning accuracy by finding the relative positions of two labels is proposed.

(iv) The structure of this paper is as follows: Section 2 presents the related research. Section 3 describes the UWB positioning method in an NLOS environment proposed in this article. Section 4 discusses the factors that affect the positioning accuracy. Section 5 describes the experiments and presents an evaluation of the framework proposed in this paper. Section 6 summarizes the research presented in this article.

## 2. Related Work

Current UWB positioning is generally divided into two categories: LOS environment and NLOS environment [18], both of which are based on angle-of-arrival (AOA) estimates. If the base station can simultaneously perform TOA estimation and direction-of-arrival (DOA) estimation, one base station is sufficient to conduct positioning.

Many research teams have achieved significant results in positioning [19]. Paper [20] proposed a UWB positioning method based on TOA-DOA joint estimation. The work in [21] proposed a three-step joint estimation algorithm. First, the threshold correlation method is used for TOA estimation. Then, the least mean square algorithm is used for joint estimation of the TOA and the difference in arrival time. Finally, the DOA estimation is obtained by improving the time difference estimation accuracy in terms of arrival. In [22], another three-step joint estimation algorithm was proposed. First, the maximum likelihood estimation algorithm is used to perform the preliminary TOA estimation, and then a further joint estimation of the TOA and the arrival time difference is performed. Finally, the time difference in terms of arrival and the geometric trigonometric cosine theorem are used to perform DOA estimation. The work in [23] proposed a two-step joint estimation algorithm, which first uses the TC algorithm to perform a rough estimation of the TOA and then uses a log-likelihood equation to find the best value to improve TOA estimation accuracy and DOA estimation. The algorithm designed in [24, 25] requires 3 steps, and the algorithm is more complex. The estimation accuracy of the algorithm in [26] is limited by the sampling frequency, namely, the Nyquist rate in GHz. In addition, the system is complex.

Regarding a multibase station and multitag positioning, many studies exist [27]. These studies either used multiple tags [28] or additional hardware [29], namely, directional antennas, for tag positioning. In the past few years, many algorithms for distinguishing NLOS states have been proposed [30]. For example, the work in [31] proposed using the kurtosis, mean excess delay (MED), and root-mean-square (RMS) delay to distinguish the NLOS environment [29]. If this algorithm uses only a single variable, then the NLOS environment cannot be correctly distinguished. If a mixed variable [32] is used, it has a good effect, but the calculation becomes complicated, and the efficiency is reduced. Paper [33] proposed an NLOS environment discrimination algorithm based on the received signal TOA, received signal strength indication (RSSI), and RMS [34]. It can be used to distinguish an NLOS environment when the actual distance is known. However, in practical applications, the distance between the reference tag and the tag to be tested cannot be known in advance, and there are too many variables; thus, the operation is complicated, and the efficiency is low. Another document [35] proposed an NLOS-based algorithm that relies on machine learning. Although this algorithm

achieves good distinction, it is too complex. In [36, 37], an NLOS-distinguishing algorithm based on the support vector machine was proposed. It performs well but is relatively complicated compared with the method presented in this paper. In practical positioning applications, the number of operations is large.

A recent work proposed that the direction of a label can be determined by using a human body to block the wireless receiver, with the signal intensity being attenuated the most. However, this solution cannot work properly in a complicated indoor environment, and in the case of an outdoor environment, there is more room for improvement. Other solutions involving human body blocking effects have been used to estimate the interference of mobile device signals. In addition, the use of additional hardware at the receiver or transmitter end to locate a tag has been shown to incur higher infrastructure costs and is neither scalable nor portable. Compared with the work mentioned above, this article uses the UWB to provide a simpler operation than the RSSI and to achieve more accurate indoor positioning. This method is inexpensive because only base stations and tags are needed; namely, additional hardware is not required.

## 3. UWB Positioning Method under NLOS

This paper proposes a positioning method based on UWB in an NLOS environment. The direction of a label is determined via direction estimation and position estimation. The positioning process is shown in Figure 1.

Direction estimation. The user is at multiple locations around the base station, as shown in Figure 2(a). From the UWB signals measured at different locations, the location that has the greatest impact on the UWB signal is analyzed and calculated. The angular range calculated at this position represents the rough direction of the label. To obtain the precise label direction, according to the rough direction determined above, the angle is slowly moved within the set error range. The angle range obtained during the first step is extended to the left and right sides, as shown in Figure 2(b). By analyzing the continuously collected UWB data, it is found that when the user moves slowly over the arc, the angle range can be narrowed down, and the exact angle of the label can be calculated.

Location estimation. First, the user can directly obtain the direction of the tag via the above method while effectively reducing the influence of the NLOS environment. The tag is in motion, causing the received signal to have more severe distortion due to the Doppler effect. Therefore, this paper uses the triangulation method to average the intersections of these straight lines obtained at multiple locations to find the position of the label. To improve the position accuracy, the pulse position modulation method is used in this paper. Pulse modulation is a discontinuous periodic pulse carrier whose amplitude, frequency, and intensity are controlled by the modulation signal and thus changed to achieve transmission of the information signals. This method allows the user to follow the direction of a signal to determine the location of a tag and to guide the user's direction of motion when encountering permanent obstacles, such as doors, walls, and buildings, to prevent permanent obstructions due to signal reflection and degradation and to solve the problem of deviation from the true direction of the label.

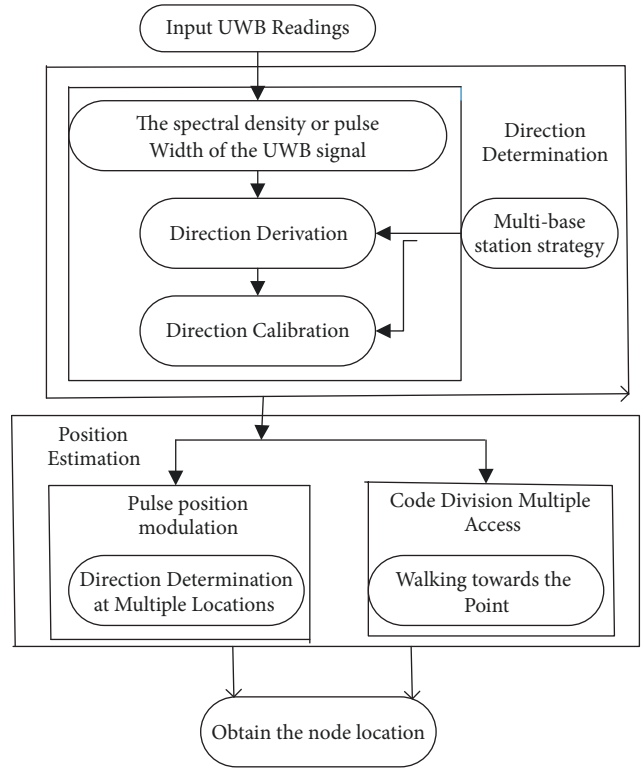


Figure 1: Framework overview.

*3.1. OVSF-TH Modulation Waveform Design.* Considering that the interference is not constant when the UWB is used for indoor positioning, the UWB waveform must be automatically adjustable according to the amount of interference, and the code resources must be fully utilizable. This article proposes an adaptive variable rate adjustment method, as shown in Figure 3.

Let the information transmission time for 1 bit $T_b$ be divided into $N_s$ frames, with the duration of each frame being $T_f$. One frame can send only one pulse. During transmission, $T_f$ can be divided into $N_c$ chip times $T_c$ for transmission, i.e., each pulse duration $T_m = T_c$. Based on this, the above process can be simply expressed as follows.

$$T_b = N_s \times T_f \tag{1}$$

Among them, $T_f = N_c T_c = N_c T_m$.

If $N_s = 8$ frames and $N_c = 3$ chips, then the OVSF spreading factor SF $= N_s = 8$.

According to the OVSF-TH coding rule, the position of the pulse in each frame is first determined according to the TH code, with each chip representing 0, 1, and 2 in sequence. Then, the position is orthogonally changed according to the OVSF code.

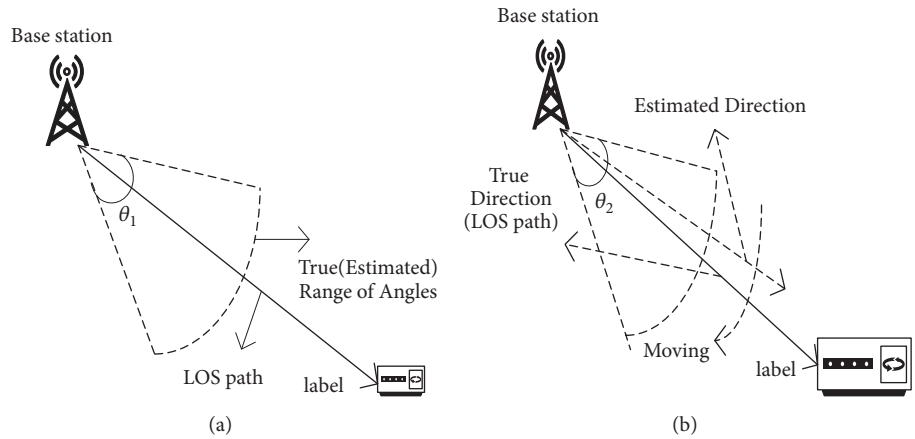


Figure 2: Illustration of direction determination. (a) Direction derivation: user stands at eight different positions around the label; (b) direction calibration: user moves across an arc that covers an angle range obtained via direction derivation.

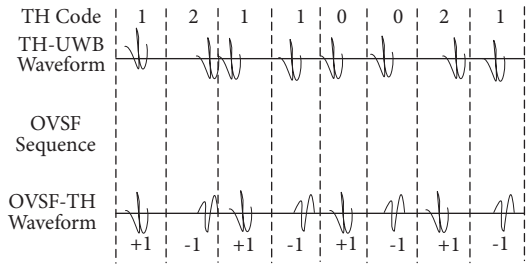


Figure 3: OVSF-TH code.

If the TH code is $c^{(k)} = \{1, 2, 1, 1, 0, 0, 2, 1\}$, then the OVSF code is $d^{(k)} = \{+1, -1, +1, -1, +1, -1, +1, -1\}$. Based on this, the signal model sent by transmitter n is as follows.

$$s^{(n)}(t) = \sum_{j=-\infty}^{+\infty} d_j^n a_{\lfloor j/N_s \rfloor}^n \sqrt{E_{TX}^n} p_0\left(t - jT_f - c_j^n T_c\right) \quad (2)$$

Among them, $a_{\lfloor j/N_s \rfloor}^n$ is the OVSF code word, the possible value of which is ±1, which represents the data flow bit. If the data flow bit is 1, then $a_{\lfloor j/N_s \rfloor}^n = +1$; otherwise, $a_{\lfloor j/N_s \rfloor}^n = -1$. $E_{TX}^n$ is the pulse energy sent by the nth user, $p_0(t)$ is the energy normalization of the pulse waveform, $c_j^n$ is the jth TH codeword of the nth user, $N_s$ is the period, and $c_j^n \in [0, N_c - 1]$ is the value range.

To analyze the OVSF-TH channel quality more intuitively, this article analyzes its bit error rate. First, define the signal received by the receiver as follows.

$$r(t) = r_u(t) + r_{mui}(t) + n(t) \quad (3)$$

Here, $r_u(t)$ is the user signal, $r_{mui}(t)$ is the multiuser same-frequency interference, and $n(t)$ is the additive white Gaussian noise (AWGN). The user $n$ sends a pulse $E_{TX}^n$, which becomes $E_{RX}^n$ after attenuation occurs. The signal loss is not considered at this time. Assuming that only user 1 sends a signal, $r_u(t)$ and $r_{mui}(t)$ are, respectively, expressed as follows.

$$r_u(t) = \sum_{j=-\infty}^{+\infty} d_j^1 a_{\lfloor j/N_s \rfloor}^1 \sqrt{E_{TX}^1} p_0\left(t - jT_f - c_j^1 T_c\right) \quad (4)$$

$$r_{mui}(t) = \sum_{N=2}^{N_s} \sum_{j=-\infty}^{+\infty} a_{\lfloor j/N_s \rfloor}^n d_j^n \sqrt{E_{RX}^n} p_0\left(t - jT_f - c_j^n T_c\right) \quad (5)$$

Since the OVSF-TH algorithm uses different spreading codes under different signal-to-noise ratio (SNR) conditions, the estimated SNR needs to be calculated at the output of the correlator. At the same time, considering that the pulse signals sent by neighboring users will cause interference affecting the receiver, the pulse positions and delays of these interference pulses are all random, which will inevitably cause an increase in the bit error rate and a decrease in the SNR. Because the solution to the bit error rate is based on the solution variance, we can start by calculating the variance of the interference pulse.

Suppose that the channel is an AWGN channel and that there is no multipath interference. In the case where synchronization is established at both the transmission and reception ends, only the signal of the receiving user 1 is considered. At this time, the output after the correlator is useful for a time in the range of $[0, T_b]$. The signal is as follows.

$$Z_u = \sum_{j=0}^{N_s-1} \int_{jT_f + c_j^1 T_c}^{jT_f + c_j^1 T_c + T_c} d_j^1 d_j^1 a_{\lfloor j/N_s \rfloor}^1 \sqrt{E_{RX}^1} \bullet \left[p_0\left(t - jT_f - c_j^1 T_c\right)\right]^2 dt \quad (6)$$

Next, consider multiuser interference $Z_{mui}$. Assuming that user 1 receives interference from user $n$, the interference signal received by the receiver can be expressed as follows.

$$mui_1^n(\tau^n) = \sqrt{E_{RX}^n} \int_0^{Tc} d_j^1 d_i^n p_0\left(t - \tau^n\right) p_0(t)\, dt \quad (7)$$

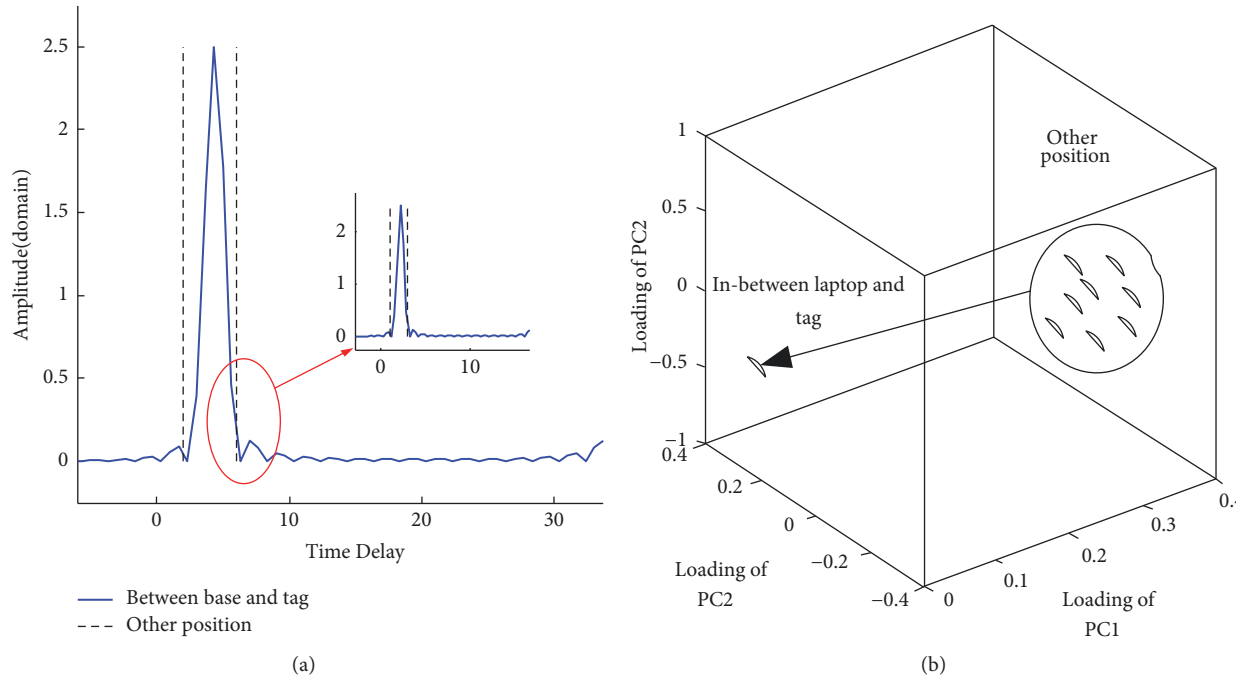


FIGURE 4: Examples of using the amplitude orthogonal transform method: (a) time domain UWB amplitudes at eight different locations around the wireless device; (b) after using the amplitude orthogonal transform method while considering the three main components.

The interference variance of user 1 from user $n$ is as follows.

$$\sigma_{bu}^2 = \frac{N_s}{T_f}\int_0^{T_f}\left(\sqrt{E_{RX}^n}\int_0^{T_c} d_j^1 d_i^n p_0(t-\tau^n)\,p_0(t)\,dt\right)^2 d\tau^n \quad (8)$$

Formula (8) is analyzed because, for any user, the distribution of delay $\tau$ is the same. Thus, for any user $n$, the value of the integral $\int_0^{T_f}(\int_0^{T_c} d_j^1 d_i^n p_0(t-\tau^n)p_0(t)dt)^2 d\tau^n$ is the same. Hence, the following can be obtained.

$$\sigma_{bu}^2 = \int_0^{T_f}\left(\int_0^{T_c} d_j^1 d_i^n p_0(t-\tau^n)\,p_0(t)\,dt\right)^2 d\tau^n \frac{N_s}{T_f}\sqrt{E_{RX}^n} = \frac{N_s}{T_f}\sqrt{E_{RX}^n} \quad (9)$$

Here, $\sigma_M^2 = \int_0^{T_f}(\int_0^{T_c} d_j^1 d_i^n p_0(t-\tau^n)p_0(t)dt)^2 d\tau^n$.

Therefore, in the case where the average of the multiuser interference and Gaussian white noise is 0 and the variance is $N_0/2$, the bit error rate of the final OVSF-TH is as follows.

$$P_{rb} = \frac{1}{2}\operatorname{erfc}\sqrt{\frac{\left(\left(2N_s\sqrt{E_{RX}^1/N_0}\right)^{-1} + \left(\left(N_s E_{RX}^1/\sigma_M^2\,(1/T)\sum_{n=2}^{N_u} E_{RX}^n\right)^{-1}\right)^{-1}}{2}} \quad (10)$$

When the bit error rate is high, the signal interference is large, and the SNR is low; when the bit error rate is low, the signal is subject to less interference, and the SNR is high. The OVSF-TH modulation method is used to calculate the bit error rate at that time using the calculation result of (9). The error rate of the current channel can be more intuitively analyzed based on the value of the bit error rate. In general, the OVSF code tree uses the highest frequency K = 2 layers and K = 3 layers; that is, 4 or 8 pulses represent 1 bit of information. In DS-UWB and TH-UWB, this value is a fixed value that does not change with the channel. This article uses the bit error rate $2 \times 10^{-2}$ as the boundary. When the rate is lower than this value, 4 pulses are used. Above this value, 8 pulses are used, and good results can be obtained.

*3.2. Direction Estimation Method.* For the NLOS environment, the direction estimation method for the spectral density and pulse-orthogonal transform is proposed.

The experiments show that the spectral densities are highly correlated with each other when the user is outside the DP between the base station and the tag. At the same time, regardless of the position of the blocking object, the UWB pulses at different positions also tend to be highly correlated, as shown in Figure 4. From the graph analysis,

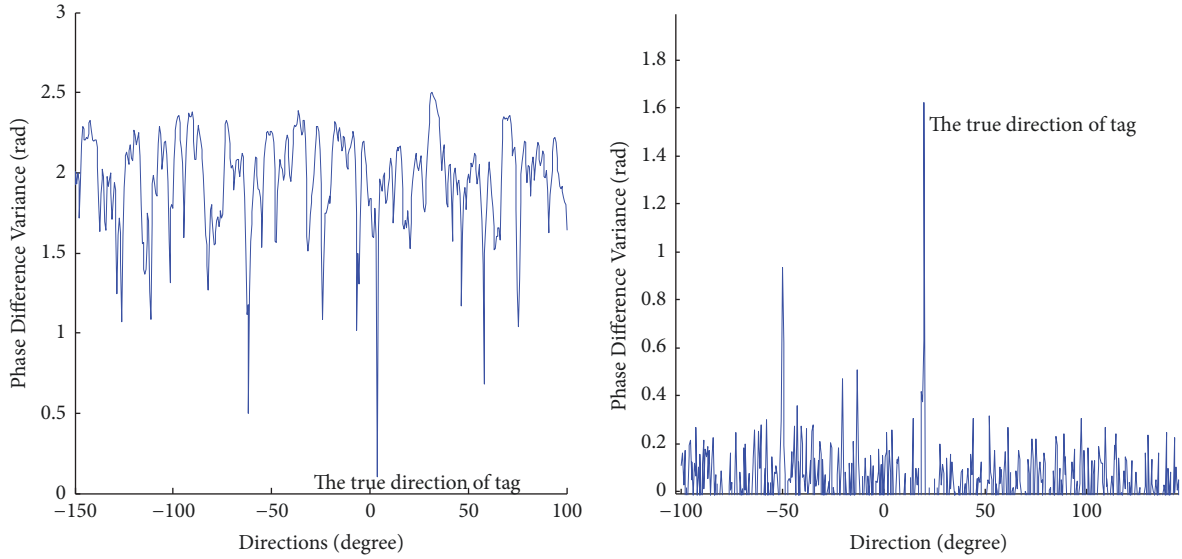


(a) Variance (b) Correlation

Figure 5: Schematic diagram of applying the pulse difference method when the user moves the laptop within a distance of 1∗0.3048 meters: (a) change in pulse position; (b) correlation coefficient of pulse position.

many reflections and refractions occur when the base station is in an open space with less reflection and far from the tag, or when the base station is in a complex indoor environment with permanent obstacles. Since the magnitude correlation method captures only rough information regarding how two sequences differ, more detailed differences are difficult to capture.

For the analysis mentioned in Figure 4, working in a simple indoor environment yields better performance. However, the analysis is very sensitive to complex indoor scenes, which can cause an increase in the number of positioning errors. To address the problems faced in complex indoor scenes, for the NLOS environment, this section uses the correlation between the two pulse-poor variances and pulse-pulley differences, utilizing the UWB pulse positions to determine the directions of tags. The UWB pulse-poor position can directly capture the blocking effect of UWB signals.

When the DP of wireless transmission is blocked by the user, the pulse difference $d_{\angle H,j^{(k)}}$ between two adjacent UWB signals varies greatly due to the received signal being from different paths, resulting in an increase in the pulse position difference, as shown in Figure 5(a). The variance of the pulse difference is defined as $\mathrm{var}(d_{\angle H,j})$ to characterize the effect of the user station on the UWB signal. The larger the variance is, the more likely the user is to block the DP of wireless transmissions. Therefore, the angular range derived for position $j$ of the maximum value of $\mathrm{var}(d_{\angle H,j})$ roughly indicates the direction in which the label is positioned.

In a complex indoor situation, walls, furniture, obstacles, etc. will produce multipath propagation, which may cause a large change in pulse position. In this case, the pulse difference is less effective in characterizing the blocking effect.

The UWB pulse difference $d_{\angle H,j^{(k)}}$ obtained at each user position $j$ is a sequence of values having a length $k-1$. As shown in Figure 5(b), each pulse difference sequence represents a specific pattern corresponding to the obstruction state. To filter the environmental impact, when no user is around the base station, the pulse difference sequence is first calculated, and then the initial pulse difference sequence is used to represent the multipath effect in the indoor environment. When the user is at a different location around the base station, it is used as a basic sequence associated with the phase sequence. By calculating the correlation between the pulse difference sequence when the user is at a different position and the sequence without the user being around the base station, the effect of the user's position on the UWB signal is reflected. When the DP between the tag and the base station is blocked, more significant changes occur in the UWB signal. Therefore, a lower correlation coefficient value is obtained. Subsequently, the standing position corresponding to the lowest association may be identified as the case in which the user is standing between the tag and the base station. Let the correlation coefficient $\rho_{i,0}$ be expressed as the correlation coefficient when the user stands at the position $i$. The detailed correlation coefficient calculation is similar to (18), with $a_i(t)$ being replaced with $d_{\angle H,j^{(k)}}$ and $a_j(t)$ being replaced with $d_{\angle H,0^{(k)}}$, which is the pulse difference when no user stands around the base station. Figure 5 illustrates the variation and correlation of the pulse difference when the user walks around, where the angular range is derived from the minimum value at position $j$ and $\rho_{i,0}$ is identified as the direction in which the tag exists.

### 3.3. Positioning Method Based on Geometric Relations

*3.3.1. Directional Calibration.* First, obtain the label angle range; then, continue to reduce the angle range, perform a directional calibration, and stop in the direction of the label.

As shown in Figure 2(b), when the user moves slowly over the arc of the angle range, the data packets can be collected in succession. The procedure is as follows:

*Step 1.* Calculate $\omega$ based on the collected $M$-groups to obtain the average value of the UWB signal and achieve higher resolution. Then, use the pulse-orthogonal transform method to calibrate the direction of the UWB pulse position.

*Step 2.* For directional calibration with the pulse difference, use the same sliding window to calculate the variance or correlation of the pulse position difference for each angle in the angle range derived based on the direction.

*Step 3.* Calculate the variance of the pulse difference at each angle. The desired label direction is the value with the smallest variance.

*Step 4.* In the direction export step, apply the above method to obtain the direction estimate for each position. The angular range increases until overlap is identified among multiple antenna pairs.

Via the above steps, the estimated angle of each antenna pair is obtained. Then, the estimated directions for all antenna pairs are averaged. Finally, the exact direction of the label is obtained.

*3.3.2. Coordinate Determination.* In this section, a coordinate-based estimation method is proposed. This method uses spatial diversity directly to determine the location of a tag. It performs direction determination at multiple locations and applies triangulation to obtain the location of a tag. Specifically, the user can find the orientation of a label at each location by placing the label in different locations.

The proposed scheme requires two inputs: the physical position at which the base station at the $i$th position is placed $(x_i, y_i)$ and the angle $\phi_i$ at which the $i$th position is generated toward the label. Then, a straight line $l_i : y = a_i x + b_i$ can be uniquely determined by two inputs, where $ai = -\tan(\phi_i)$ and $b_i = y_i + x_i \tan(\phi_i)$. Considering the different base station locations, two cases exist: (1) If the user repeats the direction determination at two different locations, then, according to our proposed research, the labels can be identified as two directional lines independently determined by the intersection $(\hat{x}_1, \hat{y}_1)$ at the two locations. (2) If the user repeats the direction determination at more than two locations, then multiple intersection points $(\hat{x}_i, \hat{y}_i), i = 1, 2, \ldots, m$, can be obtained, where $(\hat{x}, \hat{y}) = ((1/m)\sum_{i=1}^{m} \hat{x}_i, (1/m)\sum_{i=1}^{m} \hat{y}_i)$ is the total number of intersection points. Then, using our method, the position of the tag can be derived by calculating the centroid M of these intersections. Figure 6 shows an example of a geometric-relation-based method. This article shows examples of positioning tags obtained by performing direction determination at three different locations. The black dots represent the estimated positions of the tag and the centroids of the three intersections of the three directional lines.

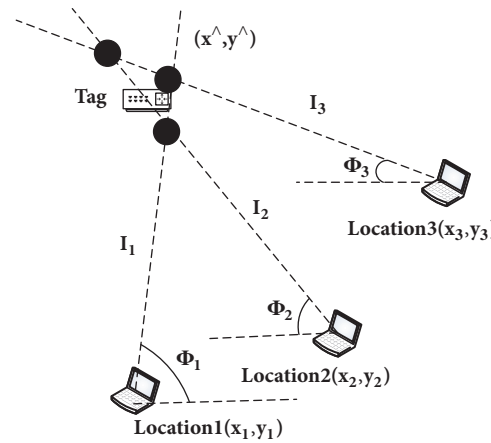


Figure 6: Geometry-relation-based methods.

When the orientation determination is performed at three different positions, the position estimation of the tag is carried out following the geometric-relation-based method. In this method, the user moves toward a tag along a certain direction and uses a single base station to reach the tag. However, the user's path may be blocked by doors, walls, buildings, etc. The user needs to bypass these obstacles and then continue approaching the rogue access point. In this case, the direction of the label passing through the obstacle must be recalculated, as the obstacle may affect the accuracy of the previous direction determination.

Users need to adjust the direction in the following two situations. In the first case, the user encounters a permanent obstacle, such as a building. The obstacle could be a dead end, such as a corner or boundary of a building. In the second case, the user performs direction determination again after traveling a long distance. In this case, the result of the previous direction determination may be inaccurate; thus, direction adjustment is also necessary.

## 4. Delay Analysis and Spatial Positioning Technology

*4.1. Time Domain Analysis in LOS Environment.* Time delays occur when the LOS is blocked. Given the UWB signal measured on each subcarrier in the frequency domain, the time domain UWB is obtained via a 60-point inverse fast Fourier transform (IFFT). The UWB signal in the time domain is described as

$$h(\tau) = \sum_{i=1}^{N} a_i e^{-j\theta_i} \sigma(\tau - \tau_i) \tag{11}$$

where $N$ is the number of multipath channel components, $a_i$, $\theta_i$, and $\tau_i$ are the amplitude of the $i$th path, the pulse position, and the propagation time delay, respectively, and $\sigma(\tau)$ is the Dirac delta function.

The graph in Figure 7 shows that when the user is at a different position, the different time delays of the UWB signal

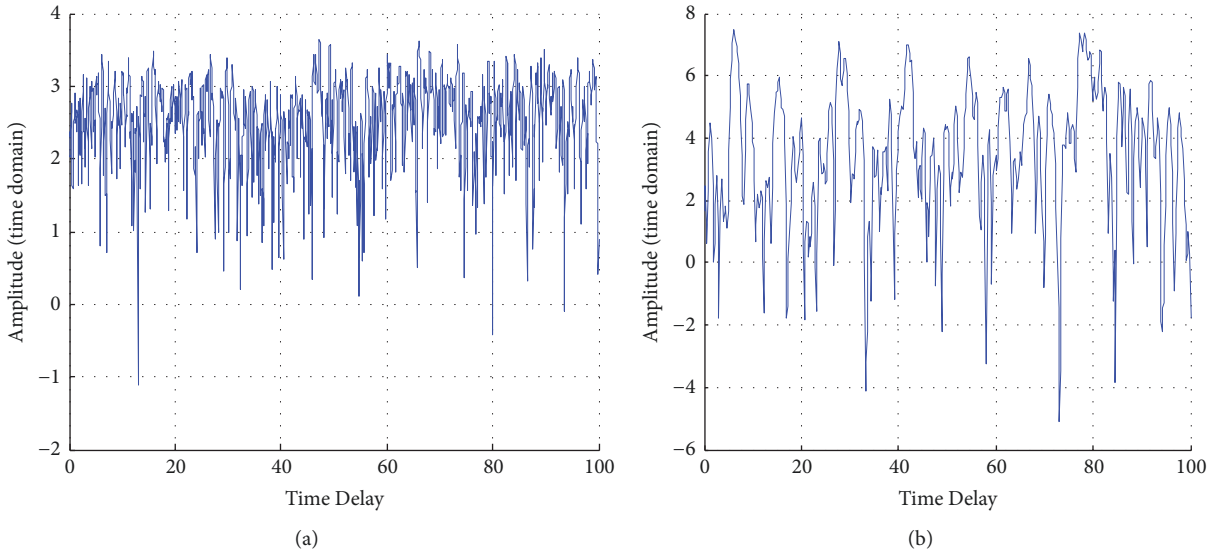


Figure 7: Time domain amplitude of UWB at eight different locations around a wireless device: time delay in a complex wireless environment.

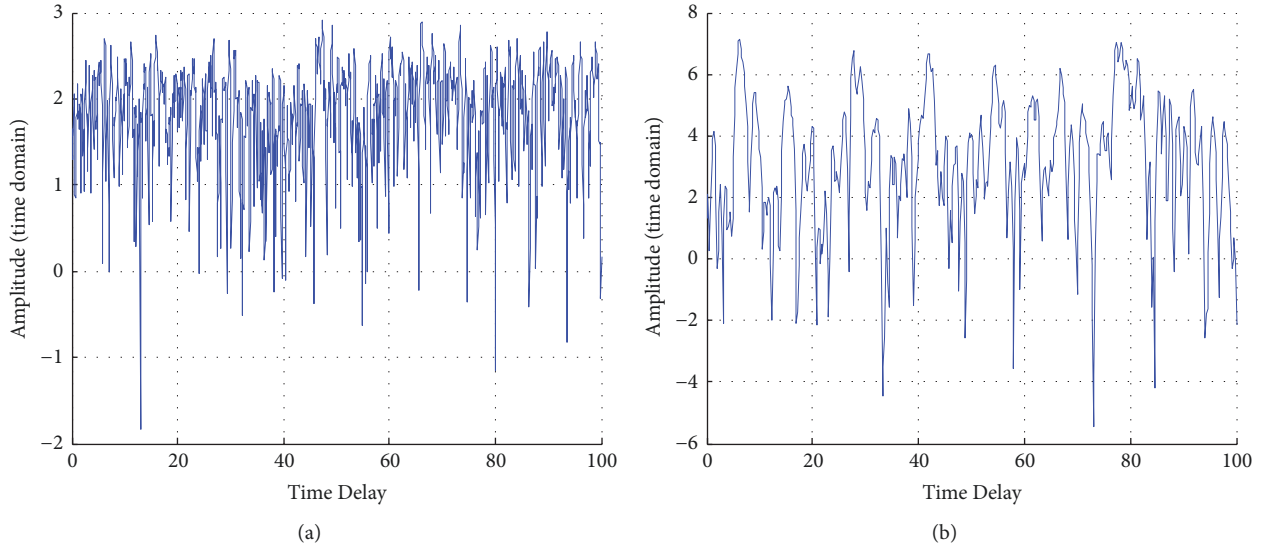


Figure 8: Time domain amplitude of UWB at eight different locations around a wireless device: time delay in a simple wireless environment.

amplitude indicate that the user is at a position such that it can block the LOS. As shown in Figure 7, the UWB signal has a plurality of time-delay amplitude peaks in the time domain. The strongest peak indicates that the UWB signal arrives via the LOS path, while a smaller amplitude peak indicates that the reflected signal follows the longer reflection path during transmission.

Furthermore, in different indoor environments, when the user is located between the base station and the tag, the strongest peak of the received signal is significantly delayed because the user blocks the DP of the signal transmission. Therefore, reflected signals transmitted along multiple paths require more time to reach the tag.

The above method performs better in the LOS environment. However, this paper finds that when no LOS exists, the delay may not be obvious in a complex indoor environment, and multipath dominates the signal propagation. Figure 8 shows no significant time delay at the strongest peak. This paper finds that this mainly occurs in a complex wireless environment; that is, there are many permanent infrastructures in the room, or there are people in the environment blocking the LOS path. Due to the complex wireless environment, the delay phenomenon may shift at smaller amplitude peaks.

To capture the time delay in simple and complex environments, the amplitude correlation is used instead of directly checking the time delay of the strongest UWB signal amplitude to determine the direction. This procedure is carried out because as long as the user does not block the DP between the base station and the tag, the UWB signal amplitudes obtained at different standing positions tend to be more

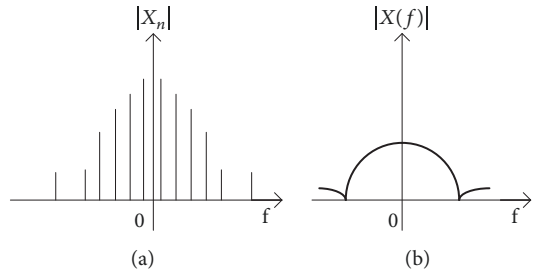


Figure 9: Amplitude diagram. (a) Magnitude frequency diagram; (b) amplitude-frequency density-frequency diagram.

correlated with each other. As shown in Figures 7 and 8, the correlation exceeds 93%. On the other hand, when the user stands between the base station and the tag, the correlation between UWB amplitude and other user locations is small, namely, less than 60%. These observations make it possible to deduce the direction of the label using the amplitude correlation at different user positions.

*4.2. Time Domain Analysis in NLOS Environment.* Spectral density information. Theoretical analysis of the spectrum obtained, for the periodic signal $x_T(t)$, is conducted using the Fourier series (*FS*) to obtain the following.

$$x_T(t) = \sum_{-\infty}^{+\infty} X_n e^{jnf_0 t} \tag{12}$$

$$X_n = \frac{1}{T}\int_0^T x_T(t)\, e^{jnf_0 t} dt \tag{13}$$

Here, $X_n$ is the spectral function of the periodic signal $x_T(t)$. In the frequency-domain coordinate system, the amplitude-frequency pattern shown in Figure 9(a) is referred to as the frequency spectrum of the periodic signal. Figure 9(b) shows that the frequency spectrum of the periodic signal is discrete and has a value only at $f = nf_0, (n = 0, \pm 1, \pm 2, \ldots)$. Its amplitude $|X_n|$ and signal $x_T(t)$ have the same dimensions, and the sum of the two spectral lines (for example, $n = \pm 3$) represents the order. The true amplitude of the spectral wave (e.g., third order) is also shown.

Aperiodic signal $x(t)$ is processed using the Fourier transform (*FT*) to obtain the following.

$$X(f) = \sum_{-\infty}^{+\infty} x(t)\, e^{jft} dt \tag{14}$$

$$x(t) = \frac{1}{2\pi}\int_{-\infty}^{+\infty} X(f)\, e^{jft} dt \tag{15}$$

$X(f)$ becomes the spectral density function of signal $x(t)$. In the frequency-domain signal coordinate system, the obtained amplitude density-frequency diagram, referred to as the signal $x(t)$ spectral density graph, is as shown in Figure 9(b). According to the graph analysis, the spectral density map of aperiodic signals is continuous. Its ordinate represents the signal's amplitude density, not the amplitude of the harmonics, and its dimension is signal dimension/Hz.

Pulse information. In the theoretical analysis of the spectrum, the pulse information:

$$H(f_k) = |H(f_k)|\, e^{j \sin(\angle H)} \tag{16}$$

where $H(f_k)$ is the channel response on the UWB signal centered at $f_k$, $|H(f_k)|$ is the amplitude, and $\angle H$ is the pulse position. The pulse position obtained from the complex value of the signal is within the range $[\pi/2, \pi/2]$. Figure 10(a) shows three consecutive packets of unpacked UWB signal phases. Clearly, when the UWB signal index increases, the UWB stage monotonically decreases, and the UWB signal is difficult to characterize by looking only at the pulse position of each packet.

Using the pulse difference to capture the blocking effect, the pulse difference between two adjacent pulses is found to be suitable for characterizing the blocking effect of UWB signals. When the user stands at position j, this paper defines the pulse difference between adjacent UWB signals k and k+1 as

$$d_{\angle H, j^{(k)}} = \left|\angle H_k - \angle H_{k+1}\right|, \quad k = 1 \ldots 29. \tag{17}$$

When the user blocks the DP between the tag and the base station, no LOS path exists, and multipath dominates the signal propagation. Therefore, the pulse difference between adjacent UWB signals is distorted, resulting in a large change in the pulse position.

In Figure 10(b), the dashed line reflects the scenario where the user stands between the laptop and the tag, while the dotted line reflects the scenario where the LOS exists. Clearly, when the user blocks the LOS path, the pulse-to-pulse difference significantly changes, while when the LOS path is not blocked, the pulse-to-pulse difference is more stable. This observation shows that changes in the pulse position can be used to capture the blocking effect. In addition, similar to the correlation of the UWB amplitude in the time domain, the correlation of the UWB pulse difference can also be used to capture the blocking effect in a complex indoor scene.

*4.3. Spatial Positioning Model.* First, the distance from the tag to the base station is obtained via measurement. Then, the three-dimensional coordinate position of the tag can be obtained according to the principle of multiball convergence. The spatial positioning model is as follows.

If Tag:(X, Y, Z), $A_0 : (X_0, Y_0, Z_0)$, $A_1 : (X_1, Y_1, Z_1)$, and $A_2 : (X_2, Y_2, Z_2)$, and if the distance from base stations $A_0$,

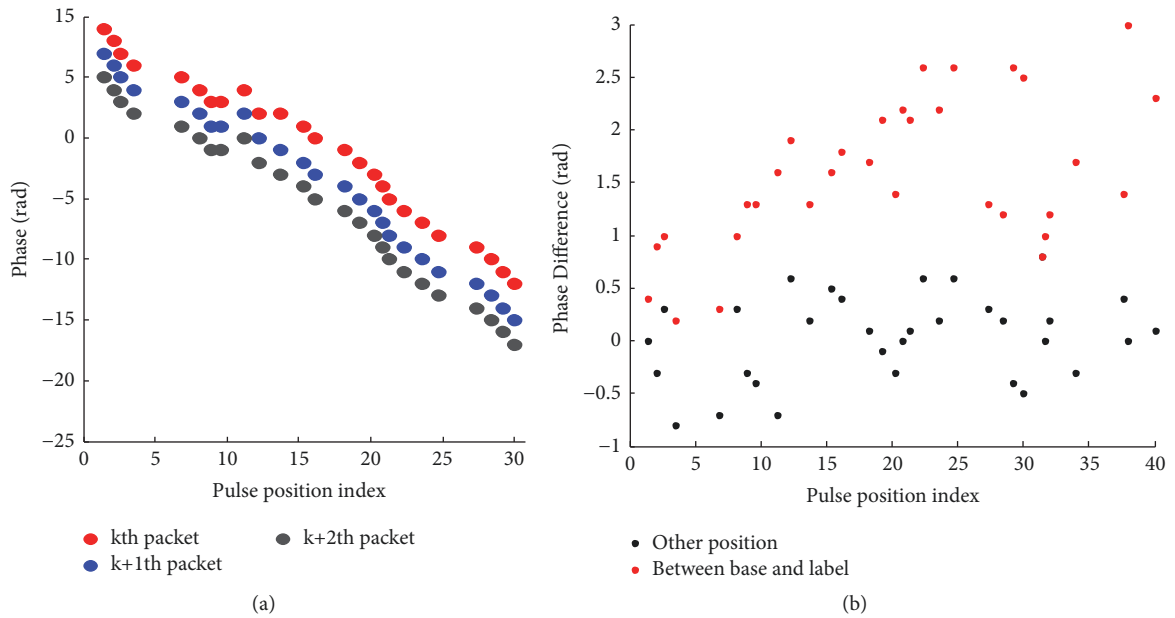


FIGURE 10: Schematic diagram of UWB pulse positions in the frequency domain: (a) pulses from three consecutive groups; (b) pulse position when the user stands at different positions.

$A_1$, $A_2$, and $A_3$ is $dis_0$, $dis_1$, $dis_2$, and $dis_3$, then you can list the ball equations for each base station and thus obtain the joint equation. The X, Y, and Z positions of the label can therefore be determined.

$$\begin{aligned}
(X_0 - X)^2 + (Y_0 - Y)^2 + (Z_0 - Z)^2 &= {dis_0}^2 \\
(X_1 - X)^2 + (Y_1 - Y)^2 + (Z_1 - Z)^2 &= {dis_1}^2 \qquad (18) \\
(X_2 - X)^2 + (Y_2 - Y)^2 + (Z_2 - Z)^2 &= {dis_2}^2
\end{aligned}$$

$$(X_1 - X)^2 + (Y_1 - Y)^2 + (Z_1 - Z)^2 = {dis_1}^2 \qquad (19)$$

$$(X_2 - X)^2 + (Y_2 - Y)^2 + (Z_2 - Z)^2 = {dis_2}^2 \qquad (20)$$

In the first step, the constants are first substituted into (21) to determine their values.

In the second step, formulas (22) to (24) are used to determine the intermediate variables. Finally, formula (20) is used to determine the real-time coordinates X, Y, and Z. Z has two results. You can remove one according to the actual situation. Therefore, when dis is updated and the second step is executed, real-time three-dimensional coordinates can be obtained.

$$\begin{aligned}
X_{10} &= X_1 - X_0, \\
Y_{10} &= Y_1 - Y_0, \\
Z_{10} &= Z_1 - Z_0 \\
X_{20} &= X_2 - X_0, \\
Y_{20} &= Y_2 - Y_0, \\
Z_{20} &= Z_2 - Z_0
\end{aligned} \qquad (21)$$

$$\begin{aligned}
A_0 &= {dis_0}^2 - XX_0^2 - Y_0^2 - Z_0^2 \\
A_1 &= {dis_1}^2 - X_1^2 - Y_1^2 - Z_1^2 \qquad (22) \\
A_2 &= {dis_2}^2 - X_2^2 - Y_2^2 - Z_2^2
\end{aligned}$$

$$\begin{aligned}
A_{10} &= -\frac{(A_1 - A_0)}{2}, \\
A_{20} &= -\frac{(A_2 - A_0)}{2}
\end{aligned}$$

$$\begin{aligned}
B_0 &= \frac{(A_{10}Y_{20} - A_{20}Y_{10})}{D}, \\
A_{20} &= \frac{(Y_{10}Z_{20} - Y_{20}Z_{10})}{D}
\end{aligned} \qquad (23)$$

$$\begin{aligned}
C_0 &= \frac{(A_{20}X_{10} - A_{10}X_{20})}{D}, \\
A_{20} &= \frac{(X_{20}Z_{10} - X_{10}Z_{20})}{D}
\end{aligned}$$

$$\begin{aligned}
D &= X_{10}Y_{20} - X_{20}Y_{10}, \\
E &= {B_1}^2 + {C_1}^2 + 1 \\
F &= B_1(B_0 - X_0) + C_1(C_0 - Y_0) - Z_0 \qquad (24) \\
G &= (B_0 - X_1)^2 + (C_0 - Y_1)^2 + {Z_0}^2 + {dis_0}^2
\end{aligned}$$

$$\begin{aligned}
X &= B_0 + B_1 * Z \\
Y &= C_0 + C_1 * Z \qquad (25) \\
Z &= \frac{\left[-F + \sqrt{F^2 - EG}\right]}{E}
\end{aligned}$$

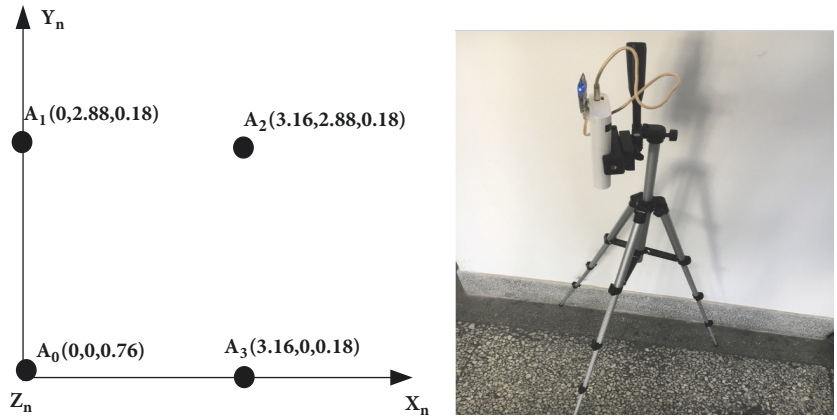


(a) (b)

Figure 11: (a) Base station space location diagram; (b) benchmark physical display.

The (X, Y, Z) obtained is the actual coordinates of the tag. Via the above method, the three-dimensional position of the target can be obtained. However, in many cases, the reliability of the positioning is expected to be higher, the accuracy is higher, or application in a wider space is desired. Therefore, more base stations need to be built, and multiple groups can be solved. More reliable and credible three-dimensional positioning data can be obtained by means of averaging, least squares, and optimal subtraction. Next, this paper uses 4 base stations to evaluate the performance of the direction export.

Four anchors are installed in a room. Anchor is abbreviated, and the coordinates represent the same three base stations.

$$\begin{aligned}
(X_0 - X)^2 + (Y_0 - Y)^2 + (Z_0 - Z)^2 &= {dis_0}^2 \\
(X_1 - X)^2 + (Y_1 - Y)^2 + (Z_1 - Z)^2 &= {dis_1}^2 \\
(X_2 - X)^2 + (Y_2 - Y)^2 + (Z_2 - Z)^2 &= {dis_2}^2 \\
(X_3 - X)^2 + (Y_3 - Y)^2 + (Z_3 - Z)^2 &= {dis_3}^2
\end{aligned} \tag{26}$$

Next, to more clearly demonstrate the use of the equation to determine a solution using actual data, the base station is placed in a space of 9 m∗6 m, with $A_0(0, 0, 0.76)$, $A_1(0, 2.88, 0.18)$, $A_2(3.16, 2.88, 0.18)$, and $A_3(3.16, 0, 0.18)$. Figure 11(a) presents a schematic diagram of the location of the base station space and (b) depicts a physical map.

Equation (26) can be solved to calculate the three-dimensional position of a label, as shown in formula (27).

$$\begin{aligned}
X &= \frac{\left({dis_1}^2 - {dis_2}^2 + 100\right)}{20} \\
Y &= \frac{\left({dis_0}^2 - {dis_1}^2 + 100\right)}{20} \\
Z &= {dis_0}^2 - X^2 - Y^2 + 1
\end{aligned} \tag{27}$$

A4 acts as a backup base station, can be used for redundant observations, and is used for backup calculations when a problem with the base station occurs. Therefore, the performance of the three base stations is clearly better than that of the positioning method.

*4.4. Complexity Analysis.* According to the algorithm description in this section, the time complexity of the algorithm is mainly composed of direction estimation, position determination, and node communication. The direction determination is a simple mathematical calculation and comparison. After determining the direction angle and the arrival time, the product is calculated. For each calculation and comparison, the time complexity is O(N). When the position is determined, in the worst case, if there is a coordinate deviation and the label is to be moved to fix the deviation, the algorithm time complexity is as follows.

$$N + (N-1) + (N-2) + \cdots + 2 + 1 = \frac{1}{2}N * (N+1) \tag{28}$$

Then its time complexity is O(N2). The deployment node is similar to the initialization node, so the time complexity of communication between nodes is O(1). In summary, the time complexity of the algorithm is as follows.

$$O(N) + O\left(N^2\right) + O(1) = O\left(N^2\right) \tag{29}$$

## 5. Numerical Results and Discussion

### 5.1. Experimental Method

*5.1.1. Experiment Setup.* This experiment uses the HP450 notebook and I-UWB positioning chip for experiments, as well as four base stations and two tags. Set up three experimental scenarios. Each experimental scene is 3 m∗3m in size, and the base station 0, the base station 1, the base station 2, and the base station 3 are arranged in a counterclockwise direction. The fixed four base stations, respectively, move the positions of the two tags, and the location information obtained by the tag movement is sent to the PC through the network interconnection of the base station tags, thereby


(a) Office (b) Meeting room (c) Laboratory

Figure 12: The testbeds: an office, a meeting room, and a laboratory.

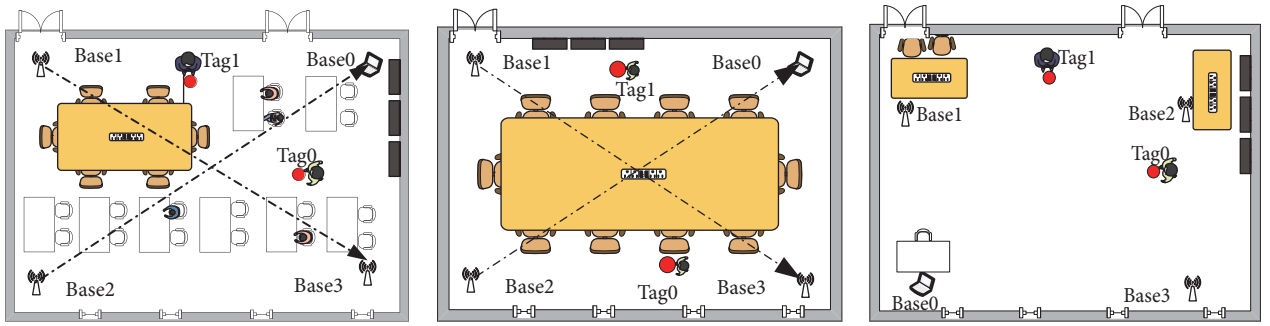


(a) Office (b) Meeting room (c) Laboratory

Figure 13: Floor plans of the testing environments.


(a) Base station (b) Power supply (c) Network diagram (d) PC-side interface

Figure 14: Hardware testbed.

obtaining the tag coordinates to further determine the positioning result. In this paper, four base stations are networked in the manner of master-slave base stations, with base station 0 as the primary base station and the remaining three base stations as the secondary base stations, which greatly reduces the time overhead of mutual communication between base stations and improves the robustness of the framework.

*5.1.2. Lab Environment.* This research conducts experiments in three indoor environments: an office, a conference room, and a laboratory. In each environment, the laptop is placed at more than 10 locations; the tags are also placed at several different locations. During the experiment, someone moves around within the environment, for example, a person walking around inside a student research lab.

A diagram of the experimental environment is shown in Figures 12 and 13.

*5.1.3. Hardware Testbed.* The hardware system used in this article is I-UWB LPS. The system has been used to obtain a single label with a 5 cm positioning accuracy. Figure 14(a) shows the positioning of the base station module and tag; Figure 14(b) depicts the power supply positioning module; Figure 14(c) presents a multinode network diagram, where the middle label is located around the four base stations; and Figure 14(d) is the PC-side serial communication interface.

*5.2. Evaluation Indicators.* This article uses the following indicators for experimental evaluation.

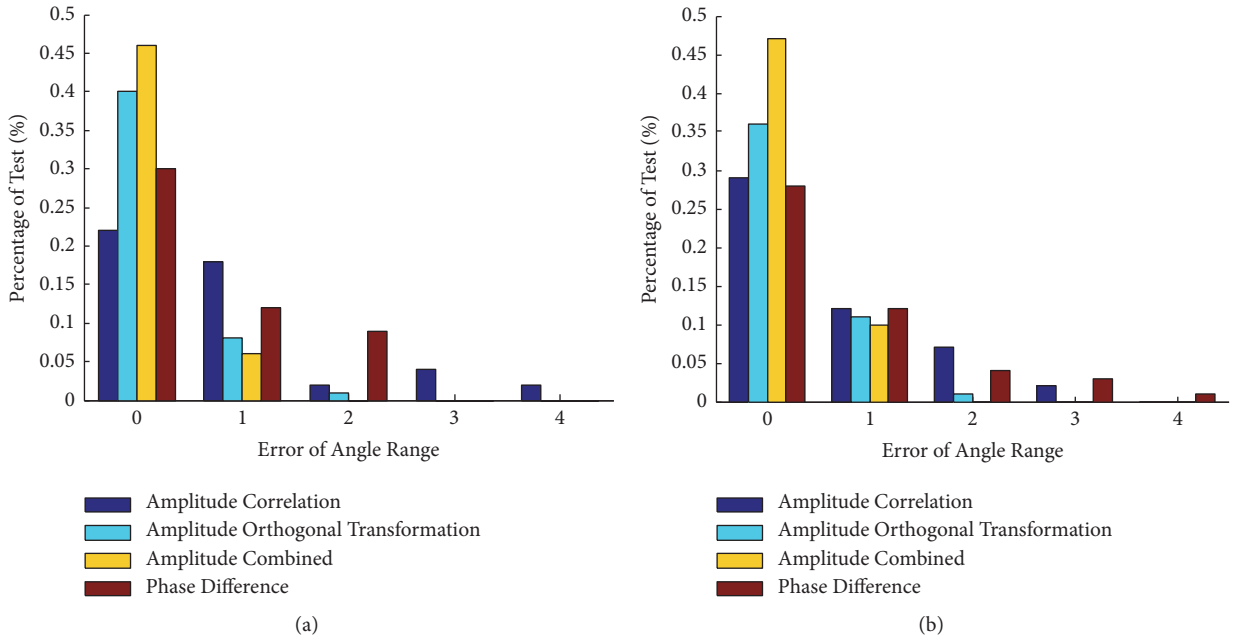


Figure 15: Direction derivation for three base stations in NLOS and LOS environments.

Angle range error. This is defined as the error between the estimated angular range and the real angular range of the label. Since 8 test positions exist around the base station, each position represents an angle range of 45 degrees. If the estimated range has a range difference with respect to the true range, the error in the angular range is 0.

Incorrect angle. This is defined as the error between the true direction of the tag and the direction of the graininess estimate, which is 1 degree.

Positioning error. This is the distance between the estimated position and the true position of the tag.

### 5.3. Performance Analysis

*5.3.1. Analysis of the Influence of the Number of Base Stations on the Accuracy.* To compare the effect of different base stations on the positioning performance, this paper carries out two sets of experiments in a real environment. First, it analyzes the comparison experiments conducted to determine the influence of the number of base stations on the positioning performance and then compares the accuracies for four base stations in three indoor environments. Figure 15 gives the performances for three base stations in terms of the positioning accuracy. Figures 16(a) and 16(b) show the performances for four base stations in terms of positioning.

Figure 15 shows that the proposed pulse combination method is effective in capturing the angular range of the indoor environment. Specifically, the pulse combination method produces a correct angular range in the case of approximately 85% under different base stations. Furthermore, the UWB pulse position difference method performs better than the UWB pulse position correlation method and is slightly inferior to the UWB pulse position orthogonal transform method in the three-base-station and four-base-station environments. The experimental results show that the pulse combination method has the best performance.

From the analysis of Figure 16, the pulse combination method integrates UWB spectral density and a pulse position orthogonal transformation. The results show that in the three-base-station and four-base-station environments, the pulse combination method can achieve the best performance in estimating the angle range of the base station. This provides a solid basis for estimating the exact angle of the base station during the directional calibration step.

*5.3.2. Performance Analysis of a Class 4 Station in Different Environments.* Experiments were performed with four base stations in three indoor environments. The experimental results are shown in Figure 17. Figure 18 shows that no large errors exist (e.g., 3 and 4) when using multiple base stations and that over 94% of the tests have an angular range error of 0 degrees. Therefore, the spatial diversity provided by multiple base stations greatly improves the overall direction derivation performance. At the same time, the number of cases where the angular range has errors is significantly reduced, especially those cases where the angular range is equal to or greater than 2, as the spatial diversity provided by a base station can mitigate the effects of severe multipath specific antenna pairs.

*5.3.3. Analysis of the Impact of Packet Size on Positioning Accuracy.* This article next examines how the number of packets used affects the performance. The numbers of packets considered in this article include 100, 500, and 1000. The results are shown in Figure 19(a). Similar results can be obtained by using the pulse correlation method, pulse combination method, pulse position orthogonal transformation, and pulse position method.

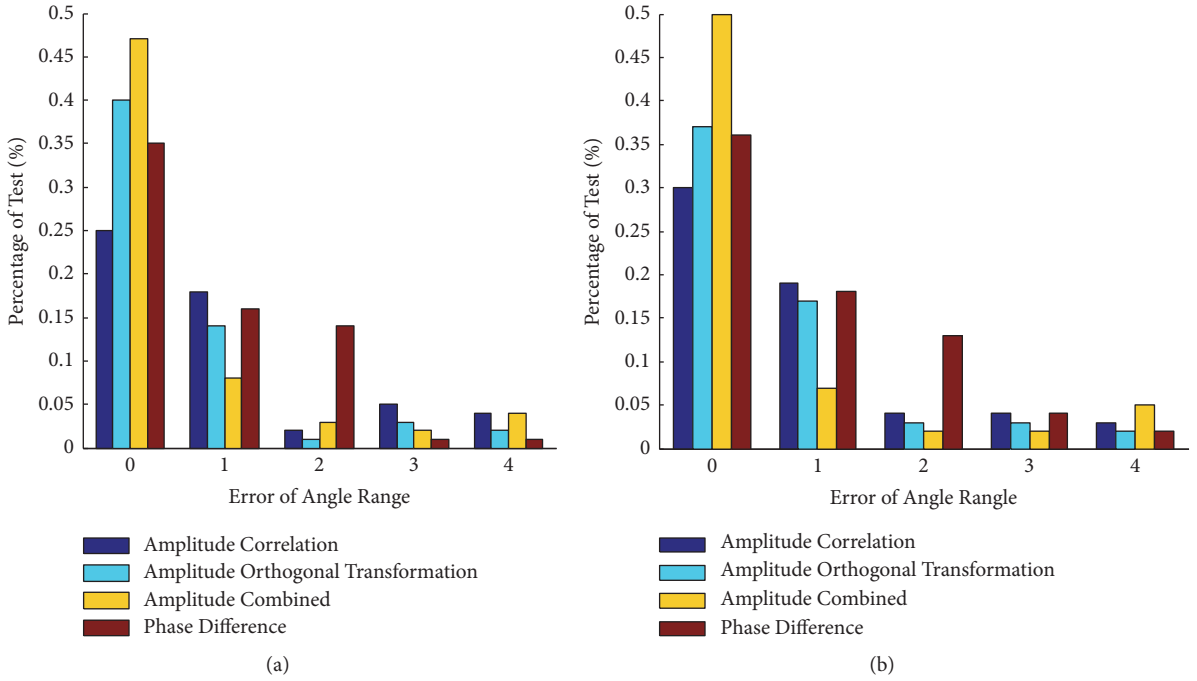


Figure 16: Direction derivation for four base stations in NLOS and LOS environments.

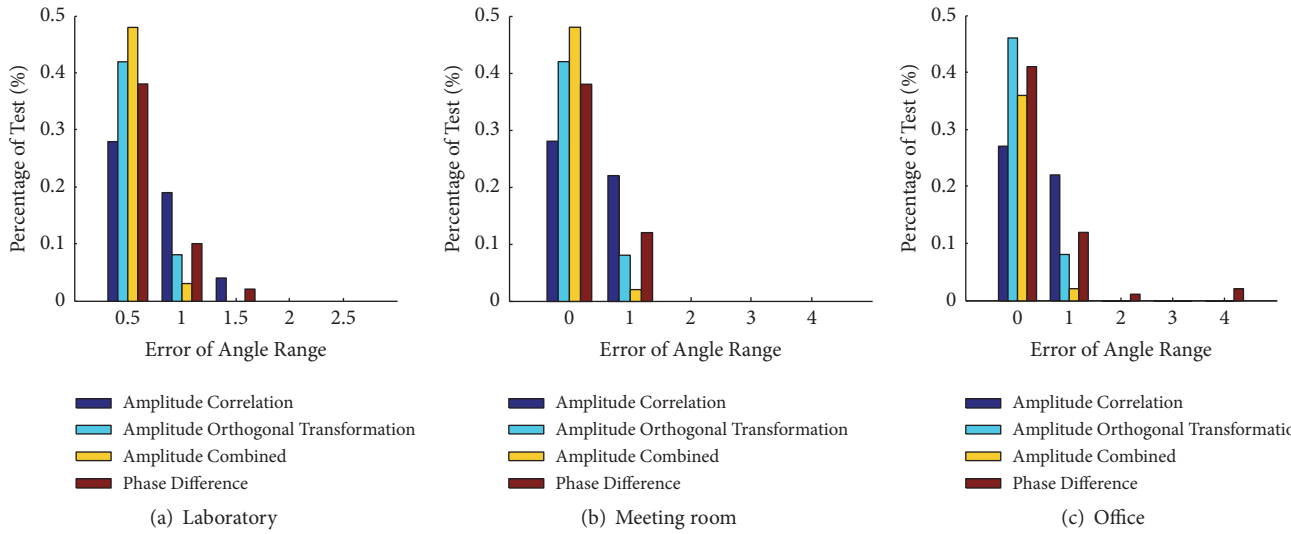


Figure 17: Direction derivation using multiple tags in indoor environments.

The experimental results show that when the number of groups used in the pulse correlation method is increased, the accuracy increases. Specifically, when the number of packets increases from 100 to 1000 packets, the percentage of the 0 angle range error increases from 78% to 93%, while for the 1 angle range error, the percentage of the angular range error decreases from 20% to approximately 5%. In addition, this paper finds that the pulse combination method is less sensitive to the number of packets. As shown in Figure 19, when the number of packets ranges from 100 to 1000, the performance of the pulse combination method does not differ greatly. Therefore, the pulse combination method can provide accurate direction derivation using only a small number of packets.

In Figure 19, this paper presents the performance in terms of the UWB spectral density and pulse direction calibration in three different indoor environments. For these three environments, the method of using the spectral density is slightly better than that of using UWB pulse positions, and the directional calibration performed via these two methods can be improved by using multiple base stations. Clearly, the proposed directional calibration achieves high accuracy in the direction of the indoor NLOS environment. Especially in the conference room, the median error is approximately 10 degrees, and the 90% error is approximately 20 degrees. The experimental results also show that the CDF curve has tails in both environments, with a maximum error of approximately 40 degrees. This result occurs mainly because

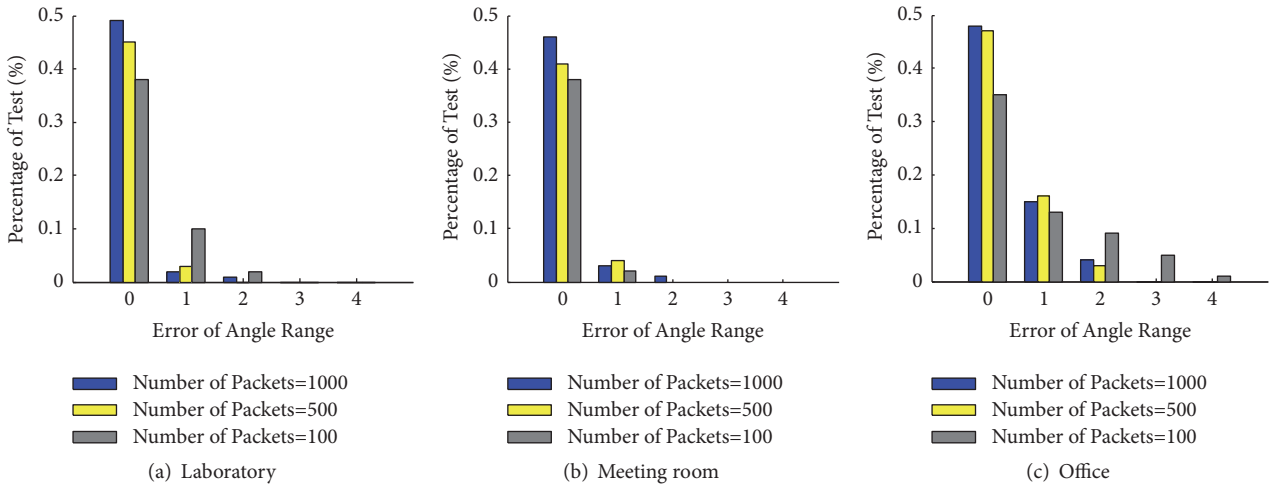


Figure 18: Impact of different numbers of packets on direction derivation using multiple tags in indoor environments.

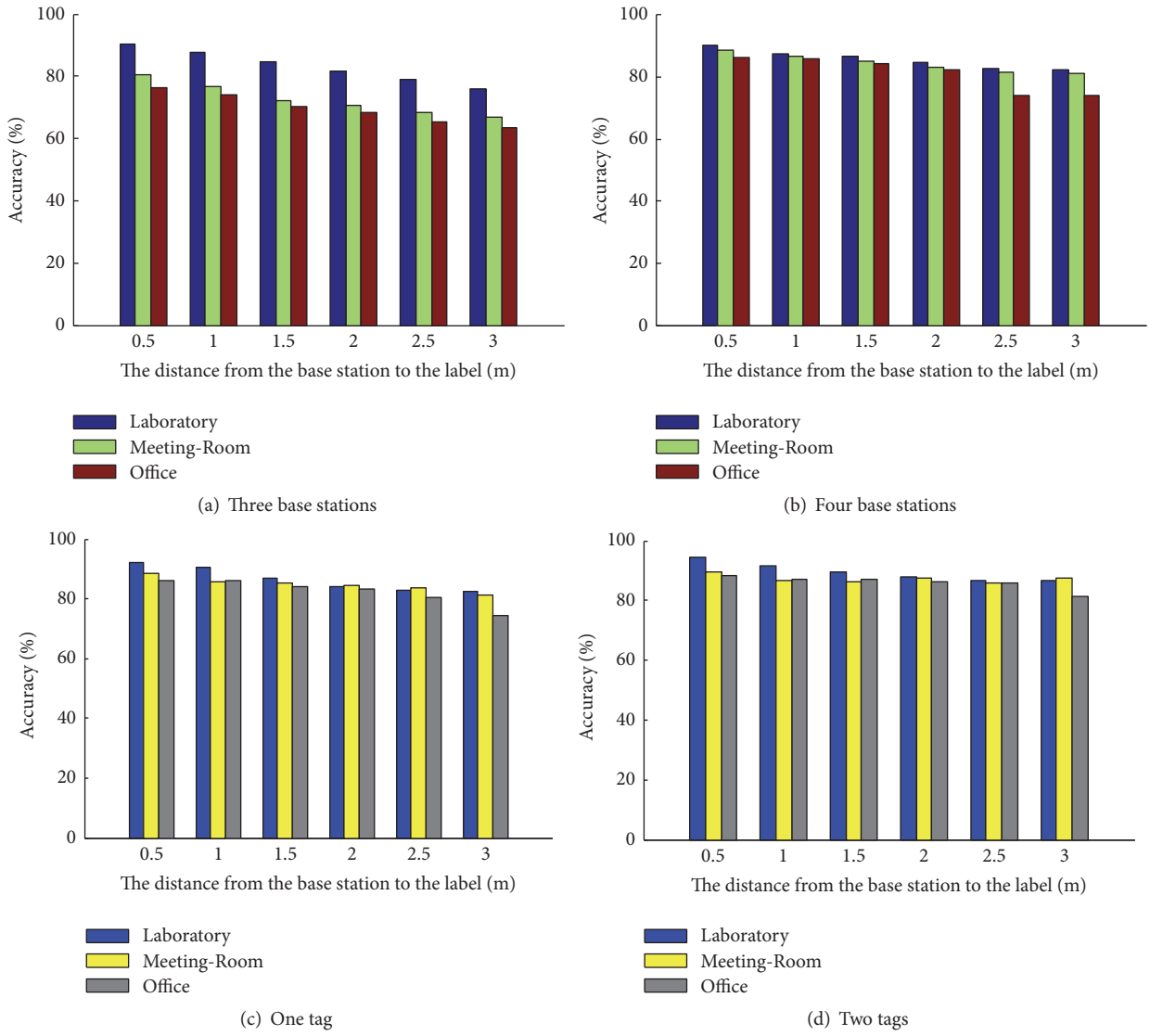


Figure 19: Accuracy of the UWB: (a) three base stations; (b) four base stations; (c) one tag; (d) two tags.

the percentage of cases in this article is very small, and errors are introduced during the direction derivation step. That is, the true direction of the label is not within the range used for calibration. In addition, the experimental results show that the LOS environment is comparable to the NLOS environment, although it is more challenging than the NLOS environment. The results show that the method in this paper is very effective whether used in a simple indoor environment or a complex indoor environment.

## 6. Conclusions

The location of a location tag is very important for ensuring the successful deployment of a pervasive wireless network. In this article, we recommend using four base stations and one tag to perform accurate tag positioning.

The single-label framework proposed in this paper involves minimal infrastructure costs and achieves high accuracy. The implementation of two procedures in the positioning framework is proposed: direction determination and position estimation. The direction determination component captures the user blocking effect on the UWB signal by exploring both the UWB spectral density and pulse positions to estimate the direction of a tag. Multiple antennas on the device can be used to further improve the direction estimation accuracy. Determining the direction of a tag can facilitate tag positioning either by using spatial diversity (determining the direction at multiple locations) to find the tag directly or by walking toward the tag by adjusting the obstacle avoidance direction. The experimental results show that the proposed UWB direction determination method is efficient and robust for indoor environments with different degrees of complexity. In contrast, the existing RSS-based angle estimation methods cannot be used indoors, and their performances outdoors are much worse than that of the method proposed in this paper. In addition, compared with the existing RSS-based methods, the UWB-based framework proposed in this paper is more efficient and accurate in locating tags. This method is shown to provide more abundant information than RSS for describing UWB signals. Further research contributions to develop precise UWB indoor positioning should be made.

## Abbreviations

| | |
|---|---|
| RSSI: | Received signal strength indication |
| CSI: | Channel state information |
| NLOS: | Non-line-of-sight |
| OVSF-TH: | Orthogonal variable spreading factor |
| UWB: | Ultra-wideband |
| TOA: | Time of arrival |
| DEMR: | Decoupled multiuser ranging |
| DP: | Direct path |
| LOS: | Line-of-sight |
| SVDD: | Support vector data description |
| DOA: | Direction-of-arrival |
| MED: | Mean excess delay |
| RMS: | Root-mean-square. |

## Data Availability

The data used to support the findings of this study are included within the article.

## Conflicts of Interest

The authors declare that they have no conflicts of interest.

## Authors' Contributions

Zhanjun Hao contributed to the algorithms and the analysis. As the supervisor of Xiaochao Dang, he proofread the paper several times and provided guidance throughout the preparation of the manuscript. Xiaochao Dang contributed to the algorithms, the analysis, and the simulations and also wrote the paper. Beibei Li and Zhanjun Hao revised the equations, helped to write the introduction and the related works, and critically revised the paper. All the authors read and approved the final manuscript.

## Acknowledgments

This work was supported by the National Natural Science Foundation of China under Grant No. 61762079 and No. 61662070; the Key Science and Technology Support Program of Gansu Province under Grant No. 1604FKCA097 and No. 17YF1GA015; and the Science and Technology Innovation Project of Gansu Province under Grant No. 17CX2JA037 and No. 17CX2JA039.

## References

[1] E. Okamoto, M. Horiba, K. Nakashima, T. Shinohara, and K. Matsumura, "Particle swarm optimization-based low-complexity three-dimensional UWB localization scheme," in *Proceedings of the 2014 Sixth International Conference on Ubiquitous and Future Networks (ICUFN)*, pp. 120–124, Shanghai, China, July 2014.

[2] M. Z. Win and R. A. Scholtz, "Characterization of ultra-wide bandwidth wireless indoor channels: A communication-theoretic view," *IEEE Journal on Selected Areas in Communications*, vol. 20, no. 9, pp. 1613–1627, 2002.

[3] D. Dardari, C. Chong, and M. Win, "Threshold-Based Time-of-Arrival Estimators in UWB Dense Multipath Channels," *IEEE Transactions on Communications*, vol. 56, no. 8, pp. 1366–1378, 2008.

[4] . Hang Ma, P. Acco, M. Boucheret, and D. Fournier-Prunaret, "Low complexity TOA estimator for multiuser DS-UWB system," in *Proceedings of the 2013 10th Workshop on Positioning, Navigation and Communication (WPNC)*, pp. 1–6, Dresden, March 2013.

[5] L. Taponecco, A. A. D'Amico, and U. Mengali, "Joint TOA and AOA estimation for UWB localization applications," *IEEE Transactions on Wireless Communications*, vol. 10, no. 7, pp. 2207–2217, 2011.

[6] S. Zhu, F. Sun, and X. Chen, "Joint UWB TOA and AOA estimation under 1-bit quantization resolution," in *Proceedings of the 2013 IEEE/CIC International Conference on Communications in China (ICCC)*, pp. 321–326, Xi'an, China, August 2013.

[7] F. Shang, B. Champagne, and I. Psaromiligkos, "A novel ML based joint TOA and AOA estimator for IR-UWB systems," in *Proceedings of the ICASSP 2013 - 2013 IEEE International Conference on Acoustics, Speech and Signal Processing (ICASSP)*, pp. 5190–5194, Vancouver, BC, Canada, May 2013.

[8] Y. Oguz and H. Kaya, "A linear signal combination model for UWB applications," in *Proceedings of the 2014 22nd Signal Processing and Communications Applications Conference (SIU)*, pp. 1459–1462, Trabzon, Turkey, April 2014.

[9] J. Khodjaev, Y. Park, and A. S. Malik, "Survey of NLOS identification and error mitigation problems in UWB-based positioning algorithms for dense environments," *Annals of Telecommunications-Annales des Télécommunications*, vol. 65, no. 5-6, pp. 301–311, 2010.

[10] M. Heidari, F. Akgul, and K. Pahlavan, "Identification of the absence of direct path in indoor localization systems," in *Proceedings of the IEEE 18th International Symposium on Personal, Indoor and Mobile Radio Communications (PIMRC '07)*, pp. 1–6, Athens, Greece, September 2007.

[11] K. Yu and Y. J. Guo, "NLOS Error Mitigation for Mobile Location Estimation in Wireless Networks," in *Proceedings of the 2007 IEEE 65th Vehicular Technology Conference*, pp. 1071–1075, Dublin, Ireland, April 2007.

[12] S. Venkatesh and R. M. Buehrer, "NLOS mitigation using linear programming in ultrawideband location-aware networks," *IEEE Transactions on Vehicular Technology*, vol. 56, no. 5, pp. 3182–3198, 2007.

[13] C.-D. Wann and C.-S. Hsueh, "NLOS mitigation with biased Kalman filters for range estimation in UWB systems," in *Proceedings of the TENCON 2007 - 2007 IEEE Region 10 Conference*, pp. 1–4, Taipei, Taiwan, October 2007.

[14] H. Mengya, D. Zhao, and H. U. Mingzhe, "Ultra-wide band technology and its development of UWB antennas," *Telecommunication Engineering*, vol. 54, no. 2, pp. 236–244, 2014 (Chinese).

[15] Z. Shijie and W. Dan, "An improved channel estimation method based on modified kalman filtering for MB UWB systems," *Telecommunication Engineering*, vol. 54, no. 5, pp. 632–636, 2014.

[16] F. Xiao, L. Chen, C. Sha et al., "Noise tolerant localization for sensor networks," *IEEE/ACM Transactions on Networking*, vol. 26, no. 4, pp. 1701–1714, 2018.

[17] F. Xiao, W. Liu, Z. Li, L. Chen, and R. Wang, "Noise-tolerant wireless sensor networks localization via multi-norms regularized matrix completion," *IEEE Transactions on Vehicular Technology*, vol. 67, no. 3, pp. 2409–2419, 2018.

[18] W. Li, T. Zhang, and Q. Zhang, "Experimental researches on an UWB NLOS identification method based on machine learning," in *Proceedings of the IEEE International Conference on Communication Technology*, 2014.

[19] M. Tabaa, C. Diou, M. El Aroussi, B. Chouri, and A. Dandache, "LOS and NLOS identification based on UWB stable distribution," in *Proceedings of the 2013 25th International Conference on Microelectronics (ICM)*, pp. 1–4, Beirut, Lebanon, December 2013.

[20] S. W. Tian, L. W. Zhao, and G. X. Li, "A support vector data description approach to NLOS identification in UWB positioning," *Mathematical Problems in Engineering*, vol. 2014, Article ID 963418, 6 pages, 2014.

[21] K. Yu and E. Dutkiewicz, "NLOS Identification and Mitigation for Mobile Tracking," *IEEE Transactions on Aerospace and Electronic Systems*, vol. 49, no. 3, pp. 1438–1452, 2013.

[22] L. Chen, X. Chen, L. Ni, Y. Peng, and D. Fang, "Human Behavior Recognition Using Wi-Fi CSI: Challenges and Opportunities," *IEEE Communications Magazine*, vol. 55, no. 10, pp. 112–117, 2017.

[23] X. Wu, Z. Tian, T. N. Davidson, and G. B. Giannakis, "Optimal waveform design for UWB radios," *IEEE Transactions on Signal Processing*, vol. 54, no. 6, pp. 2009–2021, 2006.

[24] L. Gong, W. Yang, Z. Zhou et al., "An adaptive wireless passive human detection via fine-grained physical layer information," *Ad Hoc Networks*, vol. 38, pp. 38–50, 2016.

[25] R. Zhou, X. Lu, P. Zhao, and J. Chen, "Device-free presence detection and localization with SVM and CSI fingerprinting," *IEEE Sensors Journal*, vol. 17, no. 23, pp. 7990–7999, 2017.

[26] S. Li, Z. Qin, H. Song et al., "A lightweight and aggregated system for indoor/outdoor detection using smart devices," *Future Generation Computer Systems*, 2017.

[27] O. Ammae, J. Korpela, and T. Maekawa, "Unobtrusive detection of body movements during sleep using Wi-Fi received signal strength with model adaptation technique," *Future Generation Computer Systems*, vol. 78, pp. 616–625, 2018.

[28] A. Chriki, H. Touati, and H. Snoussi, "SVM-based indoor localization in Wireless Sensor Networks," in *Proceedings of the 2017 13th International Wireless Communications and Mobile Computing Conference (IWCMC)*, pp. 1144–1149, Valencia, Spain, June 2017.

[29] C. Wu, Z. Yang, Z. Zhou, X. Liu, Y. Liu, and J. Cao, "Non-Invasive Detection of Moving and Stationary Human With WiFi," *IEEE Journal on Selected Areas in Communications*, vol. 33, no. 11, pp. 2329–2342, 2015.

[30] H. Zhu, F. Xiao, L. Sun, X. Xie, P. Yang, and R. Wang, "Robust and passive motion detection with COTS WiFi devices," *Tsinghua Science and Technology*, vol. 22, no. 4, pp. 345–359, 2017.

[31] F. Xiao, X. Xie, H. Zhu, L. Sun, and R. Wang, "Invisible cloak fails: CSI-based passive human detection," in *Proceedings of the 1st ACM Workshop on Context Sensing and Activity Recognition, CSAR 2015*, pp. 19–23, Republic of Korea.

[32] K. Qian, C. Wu, Z. Yang, Y. Liu, and K. Jamieson, "Widar: Decimeter-level passive tracking via velocity monitoring with commodity Wi-Fi," in *Proceedings of the the 18th ACM International Symposium*, pp. 1–10, Chennai, India, July 2017.

[33] L. Zhang, E. Ding, Z. Zhao, Y. Hu, X. Wang, and K. Zhang, "A novel fingerprinting using channel state information with MIMO–OFDM," *Cluster Computing*, vol. 20, no. 4, pp. 3299–3312, 2017.

[34] J. Wang, H. Jiang, J. Xiong et al., "International Conference on Mobile Computing and Networking," in *Proceedings of the International Conference on Mobile Computing and Networking*, pp. 243–256, 2016.

[35] H. Wang, D. Zhang, Y. Wang, J. Ma, Y. Wang, and S. Li, "RT-Fall: A Real-Time and Contactless Fall Detection System with Commodity WiFi Devices," *IEEE Transactions on Mobile Computing*, vol. 16, no. 2, pp. 511–526, 2017.

[36] X. Wang, L. Gao, S. Mao, and S. Pandey, "CSI-based fingerprinting for indoor localization: a deep learning approach," *IEEE Transactions on Vehicular Technology*, vol. 66, no. 1, pp. 763–776, 2017.

[37] H. Zhu, F. Xiao, L. Sun, R. Wang, and P. Yang, "R-TTWD: Robust device-free through-the-wall detection of moving human With WiFi," *IEEE Journal on Selected Areas in Communications*, vol. 35, no. 5, pp. 1090–1103, 2017.

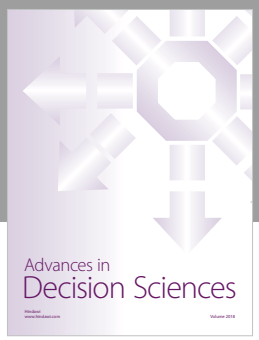

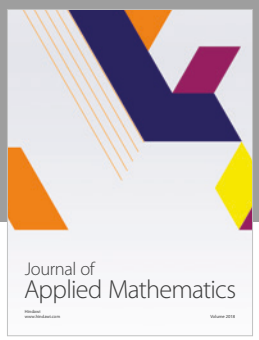

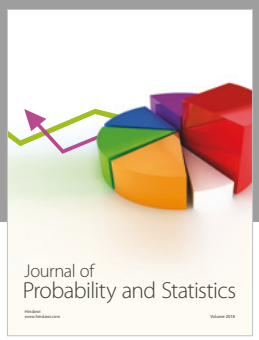

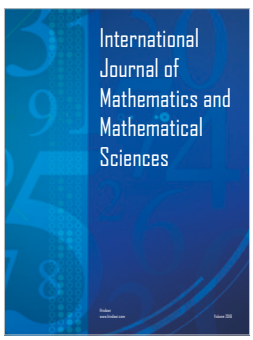

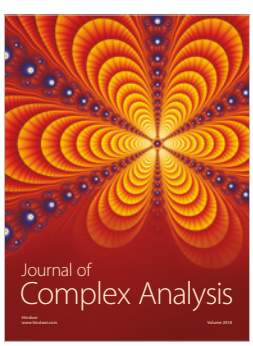

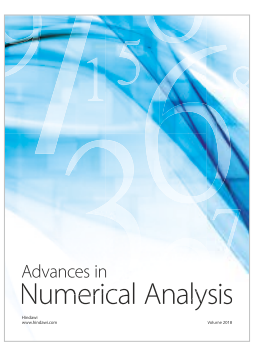

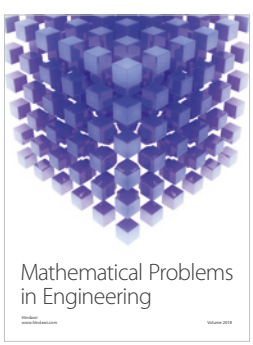

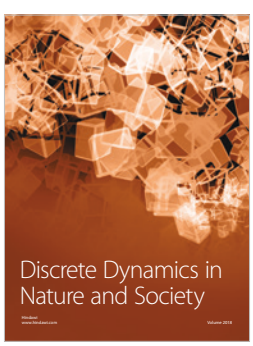

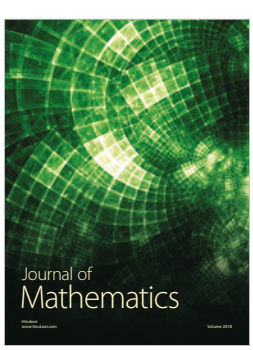

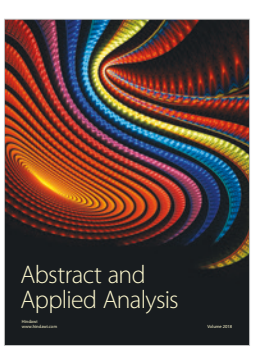

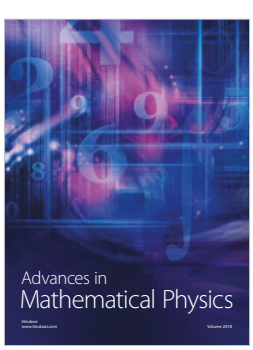

Hindawi

Submit your manuscripts at
www.hindawi.com